Making Flowers with a Penning trap: Accuracy, Resonance, and Stability

Adrian Gundersen,* Casper André Johnsen,† and Victor Berge Johansen‡

(Dated: October 22, 2025)

We study accuracy, resonance, and stability for single-, two-, and multi-Ca^+-ion systems in an ideal Penning trap. Fourth-order Runge–Kutta (RK4) is tested against the analytical solution and the forward Euler method. This shows that RK4 follows the expected global error $\mathcal{O}(h^4)$. The fitted value was ≈ 4.17 and the integrator conserves energy with a difference of $\leq 5.0 \cdot 10^{-5}\,\%$ after $T = 500\,\mu s$ with $N = 40{,}000$ time steps, proving itself to be a good tool. We also verify that the numerical scheme yields an epicyclic motion by plotting it in the xy-plane, z-values and phase-space plots. Introducing a second particle the Coulomb interactions give altered epicyclic motions showing dependency. A time-dependent drive $V_0 \mapsto V_0\big(1 + f\cos(\omega_V t)\big)$ does so certain frequencies ω_V give instability of the system as predicted by $\omega_V \approx 2\omega_z/n$. At $(\omega_+ - \omega_-)$, there is also a prominent instability region. Turning on Coulomb interactions, we find that the instability regions widen. All results can be reproduced by running the code at our GitHub repository.[a]

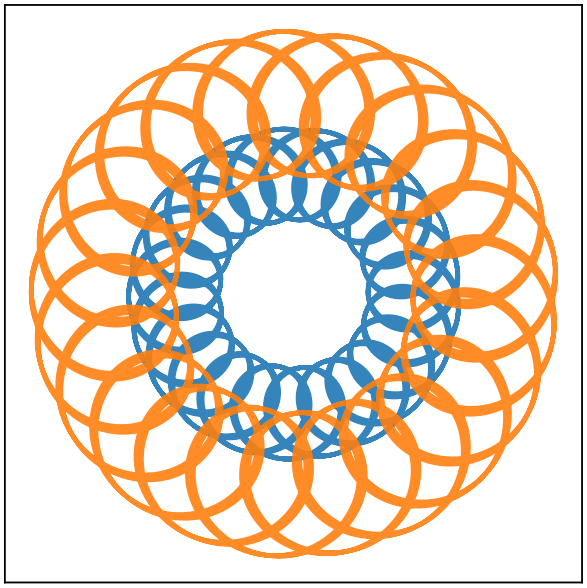

I. INTRODUCTION

Trapped, charged particles are incredibly important for many experiments and measurements. Using a homogeneous magnetic field and a quadrupole electric field, we get the Penning trap. For an idealized version of the trap, a single particle's exact solution can easily be derived. However, once we introduce a second particle, we get coupling of equations requiring numerical integration. In this article, we will look into the accuracy and convergence of numerical methods by comparing it against the known solution for a single particle.

We will then use fourth-order Runge–Kutta, to analyze the Penning trap for different parameters. Firstly, we look at a two-particle system with and without Coulomb forces, analyzing the differences in both the phase space and in xy-plane.

Finally, we look at a multi-particle system with an oscillatory term in the voltage. This we use to analyze the resonance of the system. We let the oscillatory term ω_V sweep over different values and find for which values the particles escape.

In section II we look at the physical model of the Penning trap for the different systems, discussing resonance and theoretical motion. We also formulate the numerical model with the crucial algorithms: the fourth-order Runge–Kutta, and `ACCELERATION_ALL`, returning the acceleration of all particles.

We present the results in section III with discussion rooted in the expectations from theory. Ultimately, in section IV, we provide a short summary and future implementations to improve our results. All code developed for this report is available via a GitHub repository.[a]

* adriangg@uio.no
† casjoh@uio.no
‡ victorbj@uio.no

[a] https://github.uio.no/adriangg/FYS3150

II. METHODS

Physical Model

1. The Penning trap

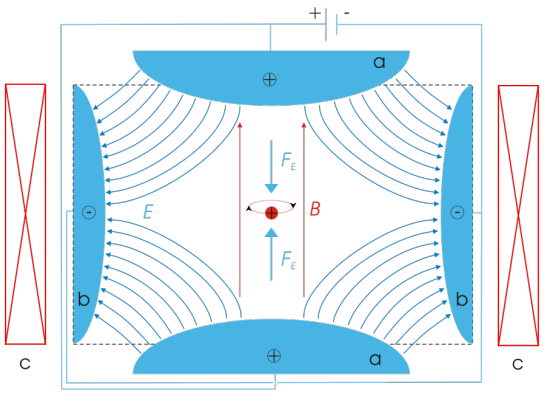

FIG. 1: Illustration of a Penning trap with a particle in the middle. The red arrows represent the magnetic **B**-field, while the blue represent the electric **E**-field. [1]

A Penning trap, as shown in Figure 1, traps charged particles using a combination of static electric and magnetic fields. The electric potential inside the trap is defined as

$$V(\mathbf{r}) = \frac{V_0}{2d^2}\left(2z^2 - x^2 - y^2\right),$$

where V_0 is the applied voltage. The characteristic trap dimension, d, denotes the distance between the electrodes. Using that the electric field $\mathbf{E} = -\nabla V$, one gets

$$\mathbf{E} = \frac{V_0}{d^2}(x, y, -2z).$$

The trap also has a magnetic field described as:

$$\mathbf{B} = B_0\hat{z}.$$

If a particle escapes the box ($\|\mathbf{r}\| > d$), we will assume that there is no electrical or magnetic field imposed on the particle.

2. Single Particle

We consider a particle of charge $q > 0$ and mass m in an ideal Penning trap. The particle experiences two forces: one from the electric field $F_E = q\mathbf{E}$, and one from the magnetic Lorentz force $F_L = q\mathbf{v} \times \mathbf{B}$, where $\mathbf{v}$ is the velocity of the particle. Newton's second law then tells us

$$\begin{aligned} m\ddot{\mathbf{r}} &= q\mathbf{E} + q\mathbf{v} \times \mathbf{B} \\ &= q\frac{V_0}{d^2}(x, y, -2z) + qB_0\mathbf{v} \times \hat{z}. \end{aligned} \tag{1}$$

Now we can look at the different components to get the full system

$$\begin{cases} m\ddot{x} = qE_x + q(\mathbf{v} \times \mathbf{B})_x = q\frac{V_0}{d^2}x + qB_0\dot{y}, \\ m\ddot{y} = qE_y + q(\mathbf{v} \times \mathbf{B})_y = q\frac{V_0}{d^2}y - qB_0\dot{x}, \\ m\ddot{z} = qE_z = -2q\frac{V_0}{d^2}z. \end{cases}$$

We define two frequencies[1]

$$\omega_0 \equiv \frac{qB_0}{m}, \quad \omega_z^2 \equiv 2\frac{qV_0}{md^2}.$$

Dividing all equations by m and inputting our frequencies, we get the following:

$$\begin{cases} \ddot{x} - \omega_0\dot{y} - \frac{1}{2}\omega_z^2 x = 0, \\ \ddot{y} + \omega_0\dot{x} - \frac{1}{2}\omega_z^2 y = 0, \\ \ddot{z} + \omega_z^2 z = 0. \end{cases}$$

However, we want to rewrite this further by introducing a complex function $f(t) = x(t) + iy(t)$. We multiply the second equation by i and add the first and second equations together.

$$\begin{aligned} \ddot{x} - \omega_0\dot{y} - \tfrac{1}{2}\omega_z^2 x + i\left(\ddot{y} + \omega_0\dot{x} - \tfrac{1}{2}\omega_z^2 y\right) &= 0 \\ (\ddot{x} + i\ddot{y}) + i\omega_0(\dot{x} + i\dot{y}) - \tfrac{1}{2}\omega_z^2(x + iy) &= 0 \\ \ddot{f} + i\omega_0\dot{f} - \tfrac{1}{2}\omega_z^2 f &= 0. \end{aligned} \tag{2}$$

This gives us a simpler differential equation for the motion in the xy-plane. The general solution to Equation 2 is given as

$$f(t) = A_+ \exp\left(-i(w_+t + \phi_+)\right) + A_- \exp\left(-i(w_-t + \phi_-)\right), \tag{3}$$

where $\phi_\pm$ are phase constants and the amplitudes ($A_\pm \in \mathbb{R}$)[2] and

$$\omega_\pm = \frac{\omega_0 \pm \sqrt{\omega_0^2 - 2\omega_z^2}}{2}.$$

To have a bounded motion in the xy-plane, the square root must be real, so that the exponents in Equation 3 are imaginary. This gives the constraint $\omega_0^2 \geq 2\omega_z^2$ as derived by Brown & Gabrielse [2]. Writing out the expressions for the frequencies, we get the requirement

$$B_0^2 \geq \frac{4mV_0}{qd^2}.$$

The distance of the particle from the origin in the xy-plane is $R(t) = |f(t)|$. Following derivation in Appendix B 1, we get that $R(t)$ is bounded at

$$R_+ = |A_+| + |A_-|, \qquad R_- = \Big||A_+| - |A_-|\Big|.$$

---

[1] In this paper we only use megahertz (MHz) to describe frequencies although we are referring to angular frequencies and rad/µs would be more precise.

[2] One could let $A_\pm \geq 0$ by letting $\phi_\pm$ absorb the sign.

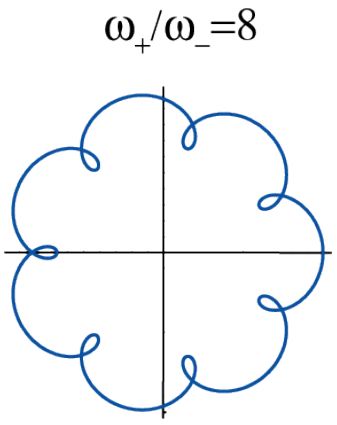

FIG. 2: Illustration of the xy-trajectory of a single particle in a Penning trap with $\omega_+/\omega_- = 8$. [3]

The two eigenfrequencies, $\omega_\pm \in \mathbb{R}$, gives the particle an *epicyclic*, "flower" motion as seen in Figure 2. The slower frequency ω_- controls the larger "orbit" in the epicycle motion, called the *magnetron motion* $A_- \exp(-i(w_- t + \phi_-))$. While the *cyclotron motion*, have the higher frequency and yields a smaller radius expressed by $A_+ \exp(-i(w_+ t + \phi_+))$.

Later, we will compare simulations to the analytical solution of the following initial value problem for a Ca^+-ion:

$$\begin{cases} \ddot{f} + i\omega_0 \dot{f} - \frac{1}{2}\omega_z^2 f = 0, \\ \ddot{z} + \omega_z^2 z = 0, \\ (x_0, y_0, z_0) = (20, 0, 20)\,\mu\text{m}, \\ (v_{x,0}, v_{y,0}, v_{z,0}) = (0, 25, 0)\,\mu\text{m}/\mu\text{s}. \end{cases} \tag{4}$$

In the xy-plane initial values plugged into (3). As $f(0) = x_0 + iy_0 = x_0$ and $\dot{f}(0) = iv_{y,0}$,

$$\begin{cases} A_\pm = \pm\frac{v_{0,y} + \omega_\mp x_0}{\omega_- - \omega_+}, \\ \phi_\pm = 0. \end{cases}$$

Putting in the values, $A_+ \approx -12.32\,\mu\text{m}$ and $A_- \approx 32.32\,\mu\text{m}$. This gives the bounds $R_- = 20.0\,\mu\text{m}$ and $R_+ = 44.65\,\mu\text{m}$.

On the z-axis we want to find a general solution with the following initial conditions:

$$\begin{cases} \ddot{z} + \omega_z^2 z = 0, \\ z(0) = z_0, \\ \dot{z}(0) = 0. \end{cases}$$

The general solution is given by:

$$z(t) = A\cos\omega_z t + B\sin\omega_z t.$$

The initial conditions then forces $B = 0$ and $A = z_0$, we then get the solution:

$$z(t) = z_0 \cos\sqrt{\frac{2qV_0}{md^2}}t. \tag{5}$$

The analytical solution for $z(t)$ Equation 5 and $f(t)$ Equation 3 will be used to validate the simulations for a single particle.

3. *Time-dependent voltage & resonance*

So far we have assumed that the voltage remains constant at V_0. However, in reality, there will be an oscillatory correction term. We let $V_0 \mapsto V_0(1 + f\cos(\omega_V t))$. We can then describe the electric field by:

$$V(\mathbf{r}, t) = (1 + f\cos(\omega_V t))\frac{V_0}{2d^2}\left(2z^2 - x^2 - y^2\right),$$

where f denotes a constant amplitude and ω_V, the angular frequency of the applied voltage. The electric field then becomes

$$\mathbf{E}(\mathbf{r}, t) = \frac{V_0}{d^2}\left(1 + f\cos(\omega_V t)\right)(x,\, y,\, -2z).$$

Having an oscillating time-dependent drive, we can assume that our system will experience resonance. We look at the new equation of motion in the z-axis.

$$\ddot{z} + \omega_z^2\left(1 + f\cos(\omega_V t)\right) z = 0.$$

Introducing

$$\delta = \omega_z^2/\omega_V^2, \quad \tau = \omega_V t, \quad \epsilon = \delta f,$$

by derivation in Appendix B 2, one obtains a version of Mathieu's equation[3]

$$\frac{d^2}{d\tau^2}z + (\delta + \epsilon\cos(\tau))\, z = 0.$$

Here, δ , is given as the polynomial

$$\delta(\epsilon) = \frac{n^2}{4} + \delta_1\epsilon + \delta_2\epsilon^2 + \ldots,$$

where the coefficients δ_i can be obtained by perturbation analysis (see, McLachlan 1947)[4]. This polynomial describes the transition curves between stable and unstable solutions of the system in a Strutt–Ince diagram[5]. Most importantly $\delta_1 = 0$, meaning for small $\epsilon = f\left(\frac{\omega_z}{\omega_V}\right)^2$, $\delta \approx \frac{n^2}{4}$, giving:

$$\delta = \frac{\omega_z^2}{\omega_V^2} \approx \frac{n^2}{4} \implies \omega_V \approx \frac{2\omega_z}{n}\,[5].$$

This means that we can expect the particles to escape the trap at these given ω_V-values. By intuition increasing the amplitude f increases the value of $f\cos\omega_V t$, which increases the range of unstable frequencies. In addition

[3] Normally written $z'' + (a - 2q\cos 2t)\, z = 0$.

it increases ϵ, thus increasing the region around δ where particles can escape. However, as we have a coupled system with eigenfrequencies $\omega_\pm$ as well, we assume more resonance frequencies. We will investigate where they are, and compare with the eigenfrequencies for a multi-particle system.

To determine if a particle is trapped we see if it satisfies $\|\mathbf{r}\| \leq d$, if $\|\mathbf{r}\| > d$, we consider it escaped and erase the particle without replacing it. After running the simulation for some time if a large fraction of particles escape we can assume that we have found a resonance frequency.

4. *Multi-particle system*

For a multi-particle system we must take into account the Coulomb force on particle i, given as

$$\mathbf{F}_{ij} = \sum_{i \neq j} k_e \frac{q_i q_j}{\left(r_{ij}\right)^3} \mathbf{r}_{ij}, \tag{6}$$

where $\mathbf{r}_{ij} = \mathbf{r}_i - \mathbf{r}_j$ is the vector between particles i and j, $r_{ij} = |\mathbf{r}_{ij}|$ its magnitude, and k_e is Coulomb's constant. Adding this to Equation 1, we get

$$m\ddot{\mathbf{r}}_i = q\mathbf{E} + q\mathbf{v} \times \mathbf{B} + \sum_{i \neq j} k_e \frac{q_i q_j}{\left(r_{ij}\right)^3} \mathbf{r}_{ij}. \tag{7}$$

There is also an interparticle magnetic force present. However, we will assume that these are negligible for our simulations as they are smaller than the Coulomb forces by $\mathcal{O}(v^2/c^2)$[6].

This gives us sufficient information to develop an algorithm that stores the accelerations of all particles as a matrix. The full steps of the algorithm can be found in Appendix C in Algorithm 2.

To get the initial positions and velocities, we initialize N particles in our box by assigning each one a random position and velocity drawn from a normal distribution. These are scaled by the characteristic dimension, d times a dimensionless factor $s_{\text{pos}}, s_{\text{vel}}$ described in Table VIII in Appendix A. These control the spread of the initial conditions. So for each particle i, we let $\boldsymbol{\xi}_i, \boldsymbol{\zeta}_i \sim \mathcal{N}(\mathbf{0}, I_3)$

$$\mathbf{r}_i(t=0) = d\, s_{\text{pos}}\, \boldsymbol{\xi}_i, \qquad \mathbf{v}_i(t=0) = d\, s_{\text{vel}}\, \boldsymbol{\zeta}_i.$$

We also find the total energy of the system. This we will use for the two-particle system to verify that RK4 is a good approximation. The total energy is given as ($E = U_{\text{tot}} + K_{\text{tot}}$)[4] where U, the potential energy, and K, the kinetic energy, is given as:

$$U_{\text{tot}} = \sum_i \left(q_i V(\mathbf{r}, t) + \sum_{j \neq i} \frac{k_e q_i q_j}{2 r_{ij}} \right), \quad K_{\text{tot}} = \sum_i \frac{m_i v_i^2}{2}. \tag{8}$$

[4] Ignoring magnetic interparticle forces.

This is implemented into TOTAL_ENERGY as described in Algorithm 4 to calculate the total energy.

Simulations

For the project, we utilized the fourth-order Runge–Kutta adapted to the Penning trap scheme. The algorithm will be accepting a PENNINGTRAP-instance (providing the equations of motion and system information) and a discrete timestep dt. A critical method from the PENNINGTRAP-class will be ACCELERATION_ALL as described in Algorithm 1 in Appendix C, giving a matrix with the acceleration of all particles. As our calculation only consists of Ca^+-ions which has consistent mass and charge, slight alterations of the algorithms given in Appendix C have been made to reduce the number cache misses and FLOPs. The constants used and the global settings for the Penning trap is to be found in Appendix A. Details on changing parameters can be found in the `README` file.[a]

We define $y(t)$, and present the mathematical formulation of the fourth-order Runge–Kutta. We then assume differential equation of the form $y'(t) = f(t, y)$. For each time step this can be solved by estimating four intermediate slopes for each step Δt It has a global truncation error of $\mathcal{O}(h^4)$. For a point (t_n, y_n) and a step size Δt:

$$\begin{aligned}
k_1 &= \Delta t\, f(t_i, y_i), \\
k_2 &= \Delta t\, f\left(t_i + \tfrac{\Delta t}{2},\, y_i + \tfrac{1}{2}k_1\right), \\
k_3 &= \Delta t\, f\left(t_i + \tfrac{\Delta t}{2},\, y_i + \tfrac{1}{2}k_2\right), \\
k_4 &= \Delta t\, f\left(t_i + \Delta t,\, y_i + k_3\right), \\
y_{i+1} &= y_i + \tfrac{1}{6}\left(k_1 + 2k_2 + 2k_3 + k_4\right).
\end{aligned}$$

For our simulations, the RK4 implementation can be found in Algorithm 3 in Appendix C. We use $y(t) = \left(\mathbf{R}(t), \mathbf{V}(t)\right)$, where $\mathbf{V}$ contains the velocities and $\mathbf{R}$, the positions of the particles. We must then evolve them at the same time.

The forward Euler algorithm, for the same differential equation, is mathematically formulated as

$$y_{i+1} = y_i + \Delta t f(t_i, y_i).$$

The theoretical global truncation error is $\mathcal{O}(h)$.

Tools

For plotting we used the Python library `matplotlib` [7], and `numpy` [8] for general calculations. We also utilized the C++ library `Armadillo` [9] for linear algebra computations.

For parallelizing our code we used OpenMP. [10] The parallelization was done for the frequency sweeps for the multi-particle system for both f and ω_V.

We also used OpenAI's ChatGPT as declared in Appendix E

III. RESULTS AND DISCUSSION

A. Comparing to the Analytical Solution

We compare Forward Euler as described in Algorithm 2 in Appendix C and fourth-order Runge–Kutta for the initial value problem given in Equation 4. The parameters are given in Appendix A. These parameters should yield stability as $\omega_0^2 \geq 2\omega_z^2$.

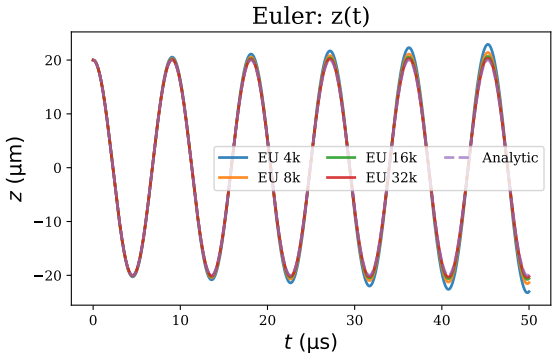

(a) Plots the Forward Euler method against analytical solution on the z-axis.

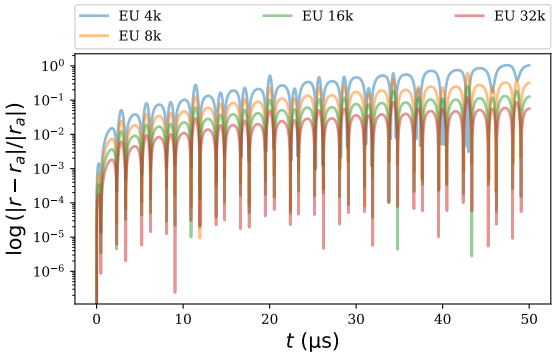

(b) Plots the relative radial error of the forward Euler method. The y-scale is logarithmic.

FIG. 3: Forward Euler vs. analytical reference. The legend corresponds to different number of iterations N, where $4k$, $8k$, ... denote $N = 4000$, 8000, and so on.

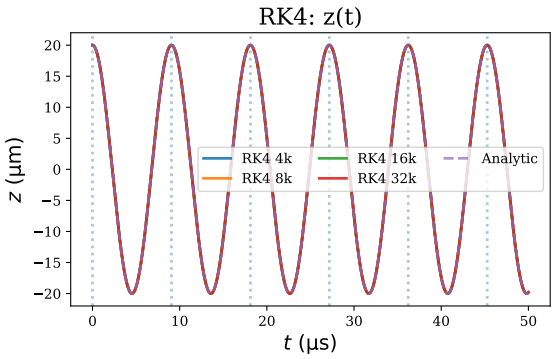

(a) Plots RK4 method against the analytical result. The x-axis displays time in microseconds, while y-axis displays z-position in micrometers. The dotted, vertical lines represent $\frac{k2\pi}{\omega_z}$, $k \in \mathbb{N}$.

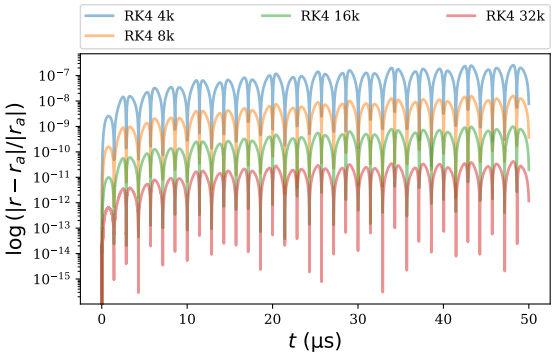

(b) Plots RK4 methods relative radial error against the analytical result. The y-axis is logarithmic.

FIG. 4: Fourth-order Runge–Kutta r vs. analytical reference r_a. The legend corresponds to different number of iterations N, where $4k$, $8k$, ... denote $N = 4000$, 8000, and so on.

In Figure 3a, we have plotted the forward Euler approximation. The deviation from the analytic solution (Equation 5) is noticeable. If we compare to the RK4 approximation in Figure 4a where multiples of the period time $T_z = \frac{2\pi}{\omega_z}$ is marked. There is no clear indication to any significant deviation. Therefore RK4 seems to be a better approach to approximate the solution.
Both Figure 4b and Figure 3b displays an oscillatory relative difference. This is most likely due to the oscillatory nature of the particle. This causes the trajectories to sometimes be closer to each other.

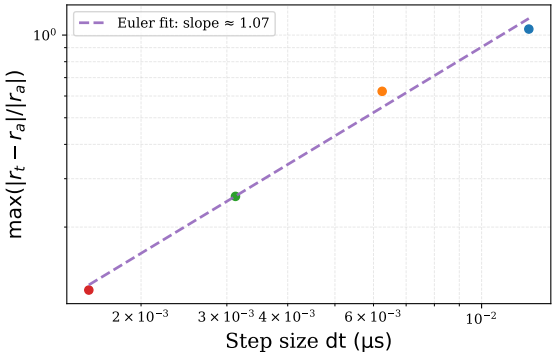

(a) Forward Euler. Slope ≈ 1.07

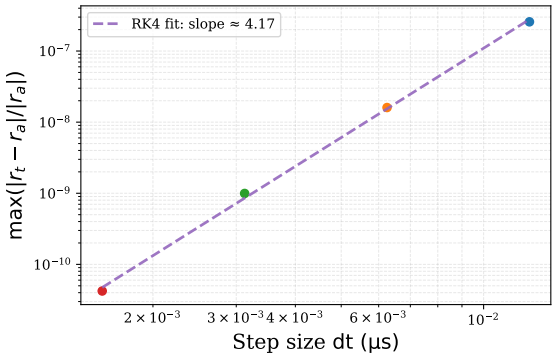

(b) Fourth-order Runge–Kutta. Slope ≈ 4.17.

FIG. 5: log–log plots of the maximum relative radial error for different step sizes $dt = \frac{T}{N}$. These are represented as points with a dotted linear regression-line fitted through them.

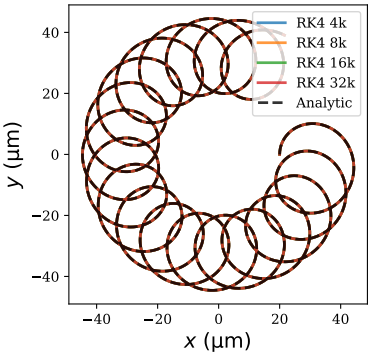

FIG. 6: The particle's motion along the xy-plane during 50 μs. The legend corresponds to different number of iterations N, where $4k$, $8k$, ... denote $N = 4000, 8000$, and so on.

The entire motion of the particle during the first 50μs is expressed in Figure 6. The magnetron and cyclotron motion is clearly visualized creating a flower pattern. Along the z-axis the particle is following the analytical sinusoidal motion (Equation 5). By contrast the forward Euler method in Figure 3a is visually drifting from the true value. Therefore, the RK4 method, with sufficiently small step sizes is the most stable method over time and will be used through the following results.

We see that for accuracy, RK4 is the clearly better choice. After 50 μs Figure 4b shows local relative errors of magnitude 10^{-14} to 10^{-7} while Figure 3b has residuals of order $\approx 10^0$. Additionally, RK4 converges faster with the slope in Figure 5b being 4.17, which implies a global error of $\approx \mathcal{O}(h^4)$, as predicted. The slope of 1.07 for the forward Euler fit from Figure 5a also holds up with the theoretical error of $\mathcal{O}(h)$.

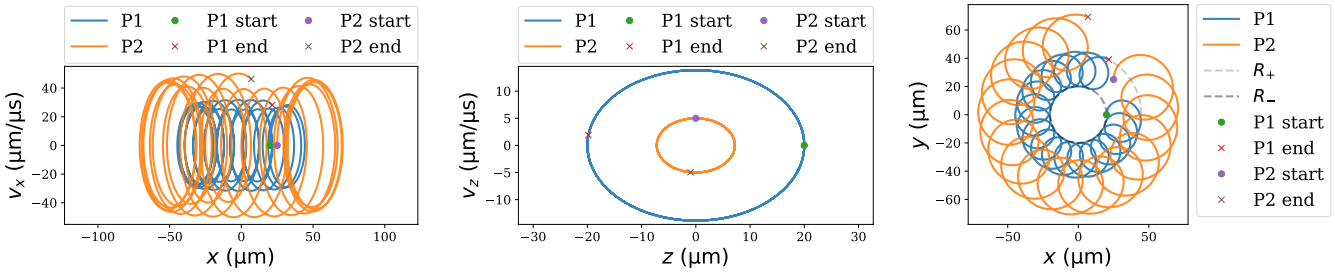

(a) x–v_x phase space (b) z–v_z phase space (c) xy-trajectory

FIG. 7: Two-particle dynamics without Coulomb interaction. Shown are projections in x–v_x, z–v_z, and xy space, respectively.

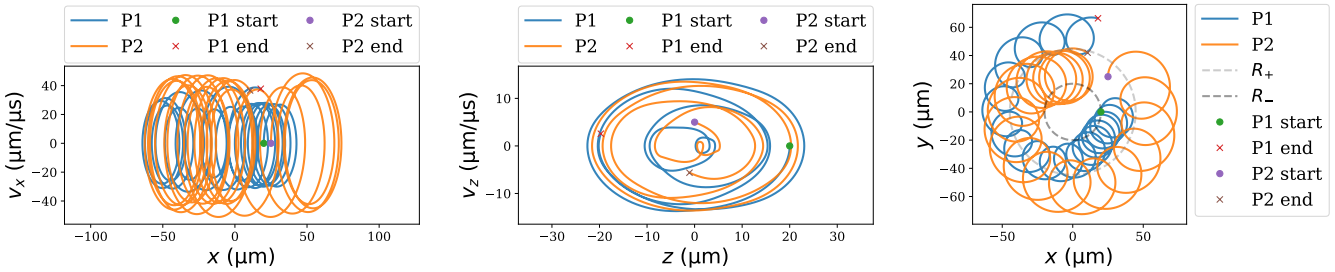

(a) x–v_x phase space (b) z–v_z phase space (c) xy-trajectory

FIG. 8: Two-particle dynamics with Coulomb interaction. The same projections without Coulomb interactions are shown as in Figure 7 for direct comparison.

B. Two-Particle Simulations

We now implement the RK4 method for a two-particle system, by adding a second Ca^+-ion with initial values:

$$\begin{cases} (x_0, y_0, z_0) = (25, 25, 0)\,\mu\text{m}, \\ (v_{x,0}, v_{y,0}, v_{z,0}) = (0, 40, 5)\,\mu\text{m}/\mu\text{s}. \end{cases}$$

We are presenting two cases. First, in Figure 7, we disabled the Coulomb interactions between the particles. These simulations are equivalent to simulating the particles individually. For instance, particle 1 follows the exact motion of the particle for the single particle in Figure 6.

By allowing the particles to interact, the trajectory changes. Both particles repel each other with the Coulomb force described in Equation 6. The orbits are now coupled and become analytically chaotic as they do not want to occupy the same space. This disturbs the flower motion so the bounds R_+ and R_- no longer hold. We see that in Figure 7c the inner particle is contained within $R(t) \in [R_-, R_+]$. However, in Figure 8c the inner particle goes outside. Also, the phase spaces in Figure 8a and Figure 8b are affected, indicating chaotic behavior.

TABLE I: The total energy in the two-particle system before and after simulation time $t = 50\,\mu\text{s}$ with $N = 40{,}000$ steps and Coulomb interactions on/off. The units are derived from our base units described in Table III in Appendix A ($[E] = (u(m/s)^2)$).

Coulomb	E_0	E_t	$\Delta E_{\text{rel}} = \frac{\lvert E_t - E_0\rvert}{\lvert E_0\rvert}$
On ($C = 1$)	45,274.76	45,274.76	0.0 %
Off ($C = 0$)	40,987.13	40,987.13	0.0 %

TABLE II: The total energy in the two-particle system before and after simulation time $t = 500\,\mu\text{s}$ with $N = 40{,}000$ steps and Coulomb interactions on/off. The units are derived from our base units described in Table III in Appendix A ($[E] = (u(m/s)^2)$).

Coulomb	E_0	E_t	$\Delta E_{\text{rel}} = \frac{\lvert E_t - E_0\rvert}{\lvert E_0\rvert}$
On ($C = 1$)	45,274.76	45,274.75	2.21×10^{-5} %
Off ($C = 0$)	40,987.13	40,987.11	4.88×10^{-5} %

After calculating the total energy of the system after 500 µs, we see that we get $< 5 \cdot 10^{-5}$ % energy loss for the system both with and without Coulomb interactions.

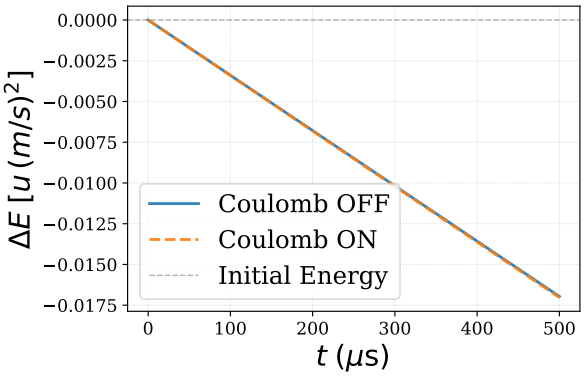

FIG. 9: Change in total energy $\Delta E = E_0 - E(t)$ for $t \in [0, 500]\,\mu s$ with $N = 40{,}000$ time steps. Both with and without Coulomb interactions are plotted. The dotted, gray line is the initial energy of the respective plots.

in Table II. This is negligible, and means that we can in good conscience utilize RK4 later for the same time $T = 500\,\mu s$ for $N = 40{,}000$ time steps without loss of stability. Figure 9 implies that the energy loss is linear and consistent. Thus, we found it unnecessary the results to an integrator like Velocity Verlet, which is designed to be energy-conserving. However, it could be beneficial for further research.

C. Multi-Particle Simulations

All the simulations were done with $N = 40000$ time steps, $N_{\text{particles}} = 100$ particles, and over $T = 500\,\mu s$. The set parameters for the frequency sweep are defined in Table VIII in Appendix A.

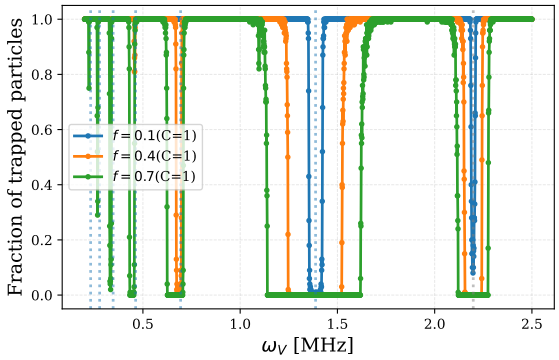

FIG. 10: Fraction of particles remaining trapped as a function of the drive frequency ω_V. $N = 100$ particles, total time $T = 500\,\mu s$, $N_{\text{steps}} = 40{,}000$, $f \in \{0.1, 0.4, 0.7\}$, $\omega_V \in [0.20, 2.50]\,\text{MHz}$ in increments of $0.001\,\text{MHz}$. Dotted lines are plotted at $2\omega_z/n \approx 1.38/n\,\text{MHz}$ for $n = 1, 2, \ldots, 6$, and $(\omega_+ - \omega_-) \approx 2.2\,\text{MHz}$.

What we notice from Figure 10 is that for the majority of the frequencies ω_V the particles are mostly contained within the trap after $500\,\mu s$. However, within a certain threshold, there are no particles in the box. This threshold increases along with f. This is expected behavior as ϵ increases, giving more δ values that are considered unstable.

Further, we want to look more closely at the resonance regions, where the particles seem to escape. We run different simulations with and without Coulomb forces. We expect resonance at $\omega_V \approx 2\omega_z/n$, where $\omega_z = 0.693893\,\text{MHz}$ in our derived units. In Figure 10 the first 6 stippled lines match the resonance regions to different degrees. Surprisingly, we observe a large resonance region around $\omega_V \approx 2.2\,\text{MHz}$. We assume this is because we did not take the eigenfrequencies $\omega_\pm$ into account.

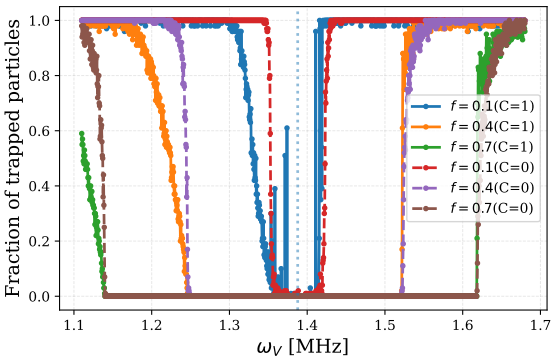

FIG. 11: $\omega_V \in [1.11, 1.68]\,\text{MHz}$ in increments of $0.0005\,\text{MHz}$. With Coulomb on and off. (Dotted line at $2\omega_z$).

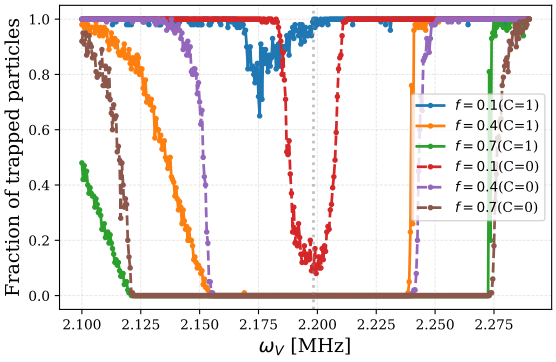

FIG. 12: $\omega_V \in [2.10, 2.29]\,\text{MHz}$ in increments of $0.0005\,\text{MHz}$. With Coulomb on and off. (Dotted line at $\omega_+ - \omega_-$).

We see that for in Figure 11, the dip seems to be centered perfectly at $\omega_V = 2\omega_z$, while the dips shift increasingly to the left compared to $\frac{2\omega_z}{n}$ for higher n's. This does

hold with the theory as $\epsilon := \frac{\omega_z^2}{\omega_V^2} f$ and as ω_V decreases, we can no longer accurately use the approximation for small ϵ. So this gives that $\omega_V^2 = \frac{4\omega_z^2}{n^2+\mathcal{O}(\epsilon^2)}$, giving a lower expected resonance region. The shift may also be due to interference with the other oscillatory eigenfrequencies.

Introducing Coulomb forces, there seems to be another overall shift towards the left. Especially, the left "shoulder" seems to stop less abrupt and take off slower. This can be seen especially in Figure 12 comparing $f = 0.4$ with (C=1) and without Coulomb interactions (C=0). At $\omega_V \approx 2.150\,\text{MHz}$ we see a much steeper takeoff without Coulomb forces. In the same figure we also see that for $f = 0.1$ there is a deeper dip without Coulomb-forces. An explanation could be that the interparticle forces change the potential energy and spread of the particles, requiring different frequencies to make the particles escape, yielding a bigger spread and a shorter dip. However, further studies would have to be done to verify this.

Although, we have not verified this theoretically, we tested *ad hoc* if the rightmost dip were centered at $\omega_V = \omega_+ - \omega_-$. Figure 12 gives strong implications that this is the case. As the equations of motion in the xy-plane are coupled this also makes intuitive sense. As $\omega_\pm$ are dependent on B_0, while ω_z one could vary the magnetic field and see if the resonance frequency follows as expected.

One could also run further simulations to get more accurate results. Running the simulations with multiple seeds and finding the average and the statistical certainty of the resonance frequency would also make it clear that it is not from statistical noise.

Other ω_V-sweeps can be found in Appendix D.

IV. CONCLUSION

In this work, we have successfully developed a numerical scheme for ions in an ideal Penning trap and validated it against theoretical groundwork. By testing it against the analytical groundwork of a single particle, we verified that fourth-order Runge–Kutta is a good numerical estimate of the mechanics of a Penning trap. For our parameters it seems to i) conserve energy sufficiently with an energy drift of $< 5 \cdot 10^{-5}\,\%$ after $500\,\mu\text{s}$, ii) converge to the analytical solution with global error $\mathcal{O}(h^4)$, and iii) be stable.

For the two-particle simulations we saw that without Coulomb-interactions the particles behaved as they were isolated. Introducing the Coulomb force affected their behavior. They no longer had perfectly circular magnetron orbits, and the inner particle was no longer bounded by R_+ and R_-. The cyclotron motion also changed, and we no longer had elliptical phase space curves. However, the conservation of energy showed the scheme could be used for multi-particle simulations.

The multi-particle simulations confirmed the hypothesis of resonance frequencies centered at $\omega_V \approx \frac{2\omega_z}{n}$. Also, for increasing amplitude f, we get a wider unstable region, as expected. We do, however, get some abnormalities in leftward shifts, but also an unexpected resonance frequency at $\omega_V \approx 2.198\,\text{MHz}$. We assume this stems from the complexity of our system not described by the simplified Mathieu equation along the z-axis.

Further work should be especially focused on the resonance findings. For instance, figuring out what causes the rightmost dip at $\omega_V \approx 2.2\,\text{MHz}$. One could potentially develop a Mathieu scheme in the xy-plane and use Floquet theory to find the expected resonances or look at superpositions of eigenfrequencies. Altering the magnetic field strength B_0 should also only shift this dip as ω_z is not dependent on the magnetic field. Also, running more simulations and calculating statistical certainty could further strengthen our findings. Implementing a velocity Verlet integrator and comparing the results may also be useful as this is energy conserving, but more demanding.

Overall, our work shows that we can utilize numerical methods to produce accurate results. This can be used to investigate and uncover mechanics not solvable analytically.

[1] Arian Kriesch. File: Penning trap.svg. https://commons.wikimedia.org/wiki/File:Penning_Trap.svg, 2006. Licensed under GFDL 1.2+, CC BY-SA 3.0, and CC BY 2.5; via Wikimedia Commons. Accessed: 2025-10-17.

[2] Lowell S. Brown and Gerald Gabrielse. Geonium theory: Physics of a single electron or ion in a penning trap. *Reviews of Modern Physics*, 58(1):233–311, 1986.

[3] jrzs. File:penningtrajec.png, 2008. Public domain, via Wikimedia Commons. Accessed: 2025-10-17.

[4] N. W. McLachlan. *Theory and Application of Mathieu Functions*, chapter III, pages 28–56. Clarendon Press, Oxford, 1947.

[5] Ivana Kovacic, Richard Rand, and Si Mohamed Sah. Mathieu's equation and its generalizations: Overview of stability charts and their features. *Applied Mechanics Reviews*, 70(2):020802, 02 2018.

[6] Anders Kvellestad. Fys3150 project 3: The penning trap. https://anderkve.github.io/FYS3150/book/projects/project3.html, 2025. Accessed: 2025-10-13.

[7] John D. Hunter. Matplotlib: A 2d graphics environment. *Computing in Science & Engineering*, 9(3):90–95, 2007.

[8] Charles R. Harris, K. Jarrod Millman, Stéfan J. van der Walt, Ralf Gommers, Pauli Virtanen, David Cournapeau, Eric Wieser, Julian Taylor, Sebastian Berg, Nathaniel J. Smith, Robert Kern, Matti Picus, Stephan Hoyer, Marten H. van Kerkwijk, Matthew Brett, Allan Haldane, Jaime Fernández del Río, Mark Wiebe, Pearu Peterson, Pierre Gérard-Marchant,

Kevin Sheppard, Tyler Reddy, Warren Weckesser, Hameer Abbasi, Christoph Gohlke, and Travis E. Oliphant. Array programming with NumPy. *Nature*, 585:357–362, 2020.

[9] Conrad Sanderson and Ryan Curtin. Armadillo: a template-based c++ library for linear algebra. *Journal of Open Source Software*, 1(2):26, 2016.

[10] OpenMP Architecture Review Board. *OpenMP Application Programming Interface*, version 5.2 edition, 2021. Accessed: 2025-10-14.

Appendix A: Parameter Tables

This appendix summarizes the constants, units, trap settings, and simulation parameters used in the report. Unless otherwise stated, times are in µs and frequencies in MHz. For each simulation set, the time step is $dt = \text{total\_time}/N$.

Code constants and units (`constants.hpp`)

TABLE III: Base and derived units used in code.

Base unit (code value)	
µm (`micrometer`)	1.0
µs (`microsecond`)	1.0
atomic mass unit m_u (`atomic_mass_unit`)	1.0
elementary charge e (`elementary_charge`)	1.0
Derived scale factors	
Tesla (`Tesla`)	9.64852558×10^1
Volt (`Volt`)	9.64852558×10^7
Coulomb constant k_e (`ke`)	$1.38935333 \cdot 10^5$
Calcium ion mass m_{Ca} (`Ca_mass`)	$40.078 \cdot m_u$

Global numerical settings and trap parameters (`parameters.hpp`)

TABLE IV: Global simulation and numerical settings.

Random seed	67
Small-r safeguard EPS	10^{-12}

TABLE V: Ideal Penning trap parameters (used unless otherwise specified). The units are derived from Table III.

Magnetic field B_0	1.0 T
Electric potential V_0	25 mV
Characteristic dimension d	500 µm
Amplitude f	0.0
Angular frequency ω_V	0.0
Coulomb interaction enabled	`true`

TABLE VI: Derived angular frequencies. The units are derived from Table III.

Derived ω_0	2.407437 MHz
Derived ω_z	0.693893 MHz
Derived ω_-	0.104539 MHz
Derived ω_+	2.302897 MHz

Simulation sets

TABLE VII: Simulation sets (`SimulationParams`).

Set	total_time T	N	dt
`single`	50.0	40000	1.25×10^{-3}
`few`	50.0	40000	1.25×10^{-3}
`multi`	500.0	40000	1.25×10^{-3}

Multi-particle setup

TABLE VIII: Multi-particle configuration and sweep parameters.

Number of particles $N_{\text{particles}}$	100
Position scale s_{pos}	0.1
Velocity scale s_{vel}	0.1
Drive amplitudes f	{0.1, 0.4, 0.7}

Appendix B: Derivations

1. Bound on radial motion

$$\begin{aligned}|f(t)|^2 &= \left(A_+ e^{-i(\omega_+ t+\phi_+)} + A_- e^{-i(\omega_- t+\phi_-)}\right)^2 \\ &= A_+^2 + A_-^2 + 2A_+A_- \cos\big[(\omega_- t+\phi_-) - (\omega_+ t+\phi_+)\big].\end{aligned}$$

Since $\cos\theta \in [-1, 1]$,

$$(|A_+| - |A_-|)^2 \;\le\; |f(t)|^2 \;\le\; (|A_+| + |A_-|)^2.$$

Taking square roots gives the bounds on the radial distance:

$$\Big||A_+| - |A_-|\Big| \;\le\; R(t) = |f(t)| \;\le\; |A_+| + |A_-|.$$

This gives bounds on the radius in the xy-plane as

$$R_+ = |A_+| + |A_-|, \qquad R_- = \Big||A_+| - |A_-|\Big|.$$

2. Mathieu equation

Let $\tau = \omega_V t$. Then $\dfrac{d^2}{dt^2} = \omega_V^2 \dfrac{d^2}{d\tau^2}$, which gives:

$$\begin{aligned}\ddot{z} + \omega_z^2\big(1 + f\cos(\omega_V t)\big)\, z &= 0, \\ \omega_V^2 \frac{d^2 z}{d\tau^2} + \omega_z^2(1 + f\cos(\tau) z &= 0, \\ \frac{d^2 z}{d\tau^2} + (\delta + \epsilon\cos(\tau))\, z &= 0.\end{aligned}$$

Appendix C: Algorithms

Algorithm 1 ACCELERATION_ALL($\mathbf{R}, \mathbf{V}, t$) for the Penning trap (from Equation 7)

procedure ACCELERATION_ALL($\mathbf{R}, \mathbf{V}$, t)
- EPS ▷ Safeguard
- $N \leftarrow$ size(trap.particles) ▷ # particles
- $\mathbf{A} \in \mathbb{R}^{3\times N}$ ▷ initialization matrix
- $\mathbf{r}_{\text{norms}} \leftarrow \big(\|\mathbf{r}_1\|_2, \ldots, \|\mathbf{r}_N\|_2\big) \in \mathbb{R}^{1\times N}$ ▷ Euclidean norms of the columns of $\mathbf{R}$
- **for** $i = 0, 1, \ldots, N-1$ **do**
  - $p_i \leftarrow$ trap.particles[i] ▷ Has charge $p.q$ and mass $p.m$
  - $\mathbf{r} \leftarrow \mathbf{R}[:, i]; \quad \mathbf{v} \leftarrow \mathbf{V}[:, i]$
  - $\mathbf{r}_{\text{norm}} = \mathbf{r}_{\text{norms}}[i]$
  - $\mathbf{E} \leftarrow$ trap.external_E_field($\mathbf{r}, \mathbf{r}_{\text{norm}}, t$)
  - $\mathbf{B} \leftarrow$ trap.external_B_field($\mathbf{r}, \mathbf{r}_{\text{norm}}$)
  - $\mathbf{F} \leftarrow p_i.q \cdot \big(\mathbf{E} + \mathbf{v} \times \mathbf{B}\big)$ ▷ Lorentz
  - $\mathbf{A}[:, i] = \mathbf{F}/p_i.m$
  - **for** $j = i+1, i+2, \ldots, N-1$ **do** ▷ Coulomb
    - $p_j \leftarrow$ trap.particles[j] ▷ Has charge $p_j.q$ and mass $p_j.m$
    - $\mathbf{r}_{ij} \leftarrow \mathbf{r} - \mathbf{R}[:, j]$
    - $r \leftarrow \max(\|\mathbf{r}_{ij}\|_2, \texttt{EPS})$
    - $\mathbf{F} \leftarrow k_e\, p_i.q \cdot p_j.q\, \frac{\mathbf{r}_{ij}}{r^3}$
    - $\begin{cases} \mathbf{A}[:, i] += \mathbf{F}/p_i.m \\ \mathbf{A}[:, j] -= \mathbf{F}/p_j.m \end{cases}$ ▷ symmetry
- **return A**

Algorithm 2 Forward Euler for the Penning trap

procedure FORWARD EULER(trap, dt, t)
- $N \leftarrow$ size(trap.particles) ▷ # of particles
- $\mathbf{r}_0, \mathbf{v}_0 \in \mathbb{R}^{3\times N}$ ▷ Current state
- $\mathbf{r}_{\text{new}}, \mathbf{v}_{\text{new}} \in \mathbb{R}^{3\times N}$ ▷ Next state
- **for** $i = 0, 1, \ldots, N-1$ **do**
  - $p \leftarrow$ trap.particles[i]
  - $\mathbf{v}_0[:, i] \leftarrow p$.velocity
  - $\mathbf{r}_0[:, i] \leftarrow p$.position
- $\mathbf{A}_0 \leftarrow$ trap.acceleration_all($\mathbf{r}_0, \mathbf{v}_0, t$)
- $\mathbf{r}_{\text{new}} \leftarrow \mathbf{r}_0 + \mathbf{v}_0\, dt$
- $\mathbf{v}_{\text{new}} \leftarrow \mathbf{v}_0 + \mathbf{A}_0\, dt$
- **for** $i = 0, 1, \ldots, N-1$ **do**
  - $p \leftarrow$ trap.particles[i]
  - p.position $\leftarrow \mathbf{r}_{\text{new}}[:, i]$
  - p.velocity $\leftarrow \mathbf{v}_{\text{new}}[:, i]$

Algorithm 3 Fourth-order Runge–Kutta for the Penning trap

procedure RK4(trap, dt, t)
$N \leftarrow$ size(trap.particles) ▷ # of particles
$\mathbf{r}_0, \mathbf{v}_0 \in \mathbb{R}^{3\times N}$ ▷ Current state

$\mathbf{r}_{\text{new}}, \mathbf{v}_{\text{new}} \in \mathbb{R}^{3\times N}$ ▷ Next state

for $i = 0, 1, \ldots, N-1$ **do**
$p \leftarrow$ trap.particles[i]
$\mathbf{v}_0[:, i] \leftarrow p$.velocity
$\mathbf{r}_0[:, i] \leftarrow p$.position

$\mathbf{k}_{r1}, \mathbf{k}_{r2}, \mathbf{k}_{r3}, \mathbf{k}_{r4} \in \mathbb{R}^{3\times N}$
$\mathbf{k}_{v1}, \mathbf{k}_{v2}, \mathbf{k}_{v3}, \mathbf{k}_{v4} \in \mathbb{R}^{3\times N}$

$\mathbf{A}_1 \leftarrow$ trap.acceleration_all($\mathbf{r}_0, \mathbf{v}_0, t$)
$\mathbf{k}_{r1} \leftarrow \mathbf{v}_0 dt \quad \mathbf{k}_{v1} \leftarrow \mathbf{A}_1 dt$

$\mathbf{r}_2 \leftarrow \mathbf{r}_0 + \frac{1}{2}\mathbf{k}_{r1}; \quad \mathbf{v}_2 \leftarrow \mathbf{v}_0 + \frac{1}{2}\mathbf{k}_{v1}$
$\mathbf{A}_2 \leftarrow$ trap.acceleration_all($\mathbf{r}_2, \mathbf{v}_2, t + \frac{1}{2}dt$)
$\mathbf{k}_{r2} \leftarrow \mathbf{v}_2 dt; \quad \mathbf{k}_{v2} \leftarrow \mathbf{A}_2 dt$

$\mathbf{r}_3 \leftarrow \mathbf{r}_0 + \frac{1}{2}\mathbf{k}_{r2}; \quad \mathbf{v}_3 \leftarrow \mathbf{v}_0 + \frac{1}{2}\mathbf{k}_{v2}$
$\mathbf{A}_3 \leftarrow$ trap.acceleration_all($\mathbf{r}_3, \mathbf{v}_3, t + \frac{1}{2}dt$)
$\mathbf{k}_{r3} \leftarrow \mathbf{v}_3 dt; \quad \mathbf{k}_{v3} \leftarrow \mathbf{A}_3 dt$

$\mathbf{r}_4 \leftarrow \mathbf{r}_0 + \mathbf{k}_{r3}; \quad \mathbf{v}_4 \leftarrow \mathbf{v}_0 + \mathbf{k}_{v3}$
$\mathbf{A}_4 \leftarrow$ trap.acceleration_all($\mathbf{r}_4, \mathbf{v}_4, t + dt$)
$\mathbf{k}_{r4} \leftarrow \mathbf{v}_4 dt; \quad \mathbf{k}_{v4} \leftarrow \mathbf{A}_4 dt$

$$\mathbf{r}_{\text{new}}[:, i] \leftarrow \mathbf{r}_0 + \frac{\mathbf{k}_{r1} + 2\mathbf{k}_{r2} + 2\mathbf{k}_{r3} + \mathbf{k}_{r4}}{6}$$
$$\mathbf{v}_{\text{new}}[:, i] \leftarrow \mathbf{v}_0 + \frac{\mathbf{k}_{v1} + 2\mathbf{k}_{v2} + 2\mathbf{k}_{v3} + \mathbf{k}_{v4}}{6}$$

for $i = 0, 1, \ldots, N-1$ **do**
$p \leftarrow$ trap.particles[i]
p.position $\leftarrow \mathbf{r}_{\text{new}}[:, i]$
p.velocity $\leftarrow \mathbf{v}_{\text{new}}[:, i]$

Algorithm 4 TOTAL_ENERGY() $E = U_{\text{tot}} + K_{\text{tot}}$ (from Equation 8)

procedure TOTAL_ENERGY
- EPS ▷ Safeguard
- $N \leftarrow$ size(trap.particles) ▷ # particles
- $\mathbf{K} \in \mathbb{R}^{1\times N}$ ▷ initialization vector kinetic energy
- $\mathbf{U}_E \in \mathbb{R}^{1\times N}$ ▷ initialization vector electrical potential
- $\mathbf{U}_c \in \mathbb{R}^{1\times N}$ ▷ initialization vector Coulomb potential
- **for** $i = 0, 1, \ldots, N-1$ **do**
  - $p_i \leftarrow$ trap.particles[i] ▷ Has charge $p.q$ and mass $p.m$
  - $\mathbf{K}[i] = \frac{1}{2} m \mathbf{v}^2$
  - $\mathbf{U}_E[i] = \frac{p_i.q \cdot}{2d^2} V(\mathbf{r}_i, t)$
- **if** coulomb_on **and** $N > 1$ **then**
  - **for** $i = 0, 1, \ldots, N-1$ **do**
    - **for** $j = i+1, i+2, \ldots, N-1$ **do** ▷ Coulomb
      - $p_i \leftarrow$ trap.particles[i] ▷ Has charge $p.q$ and mass $p.m$
      - $p_j \leftarrow$ trap.particles[j] ▷ Has charge $p_j.q$ and mass $p_j.m$
      - $\mathbf{r}_{ij} \leftarrow \mathbf{r_i} - \mathbf{r_j}$
      - $r \leftarrow \max(\|\mathbf{r}_{ij}\|, \text{EPS})$
      - $U \leftarrow k_e \, p_i.q \cdot p_j.q \, / r$
      - $\mathbf{U}_c[i] = \frac{1}{2} U$
      - $\mathbf{U}_c[j] = \frac{1}{2} U$
- **return** $\mathbf{K} + \mathbf{U}_c + \mathbf{U}_E$ ▷ For total energy of the system you must sum all components

Appendix D: ω_V-sweeps

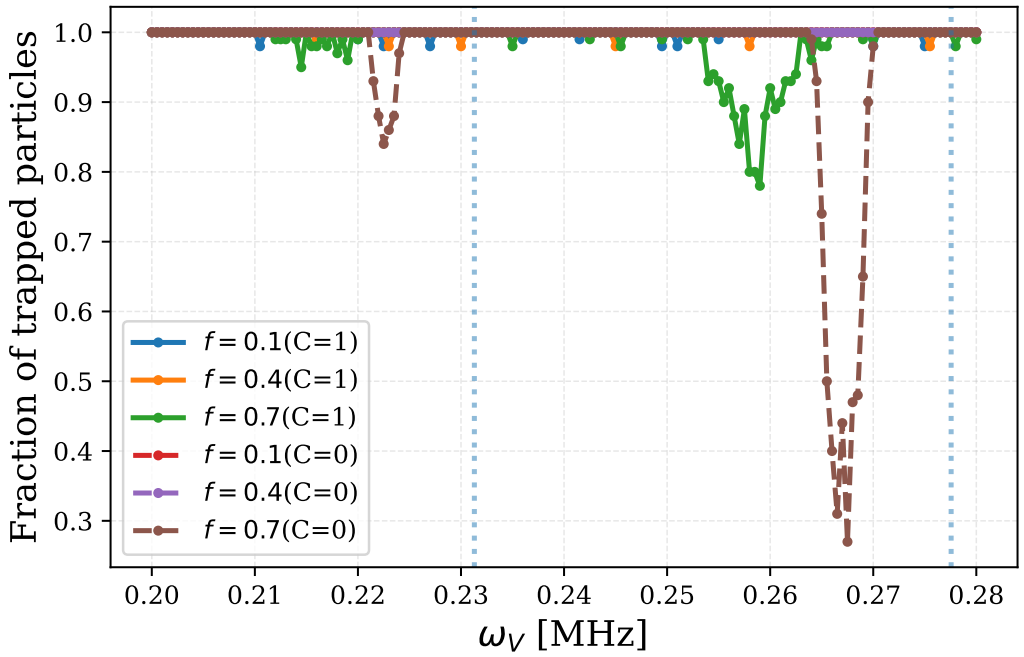

FIG. 13: $\omega_V \in [0.2, 0.28]$ MHz in increments of 0.0005 MHz. With Coulomb on and off. The dotted lines are at $\frac{2\omega_z}{6}$ and $\frac{2\omega_z}{5}$

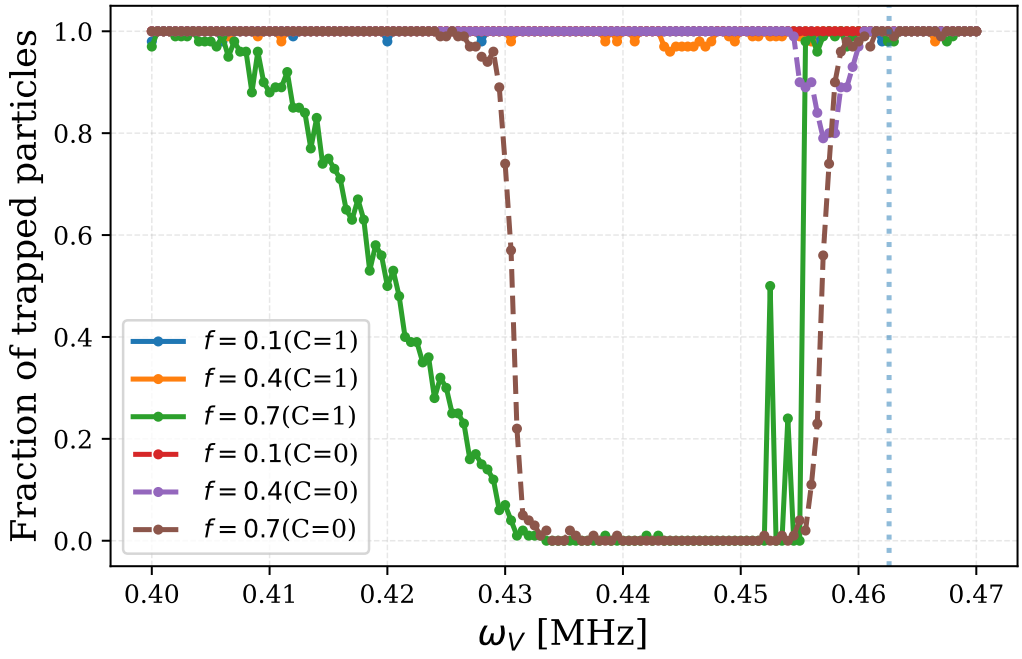

FIG. 14: $\omega_V \in [0.4, 0.47]$ MHz in increments of 0.0005 MHz. With Coulomb on and off.

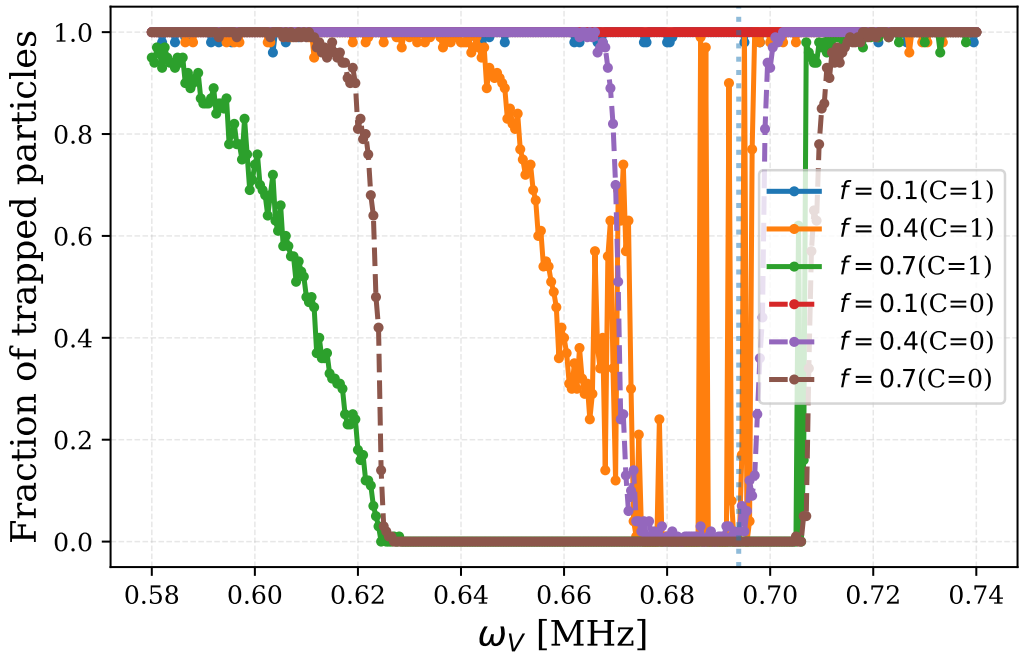

FIG. 15: $\omega_V \in [0.58, 0.74]$ MHz in increments of 0.0005 MHz. With Coulomb on and off.

Appendix E: Declaration of Use of Generative AI

In this scientific work, generative artificial intelligence (AI) has been used. All data and personal information have been processed in accordance with the University of Oslo's regulations, and we, as the authors of the document, take

full responsibility for its content, claims, and references. An overview of the use of generative AI is provided below.

Summary

- **Tool(s) used:** OpenAI ChatGPT (GPT-5), https://chatgpt.com/
- **Use:**
  - Generating boilerplate code like plotting with `matplotlib`.
  - Generating Makefiles.
  - Formatting README.md.
  - Checking language for clarity and grammar and general proof reading.
  - Generating brief code documentation, comments, and variable names for better readability in adherence to conventions.
  - Creating tables in proper tex-format.
  - Brainstorming ideas for optimizing code for efficiency.